IOP Conf. Series: Journal of Physics: Conf. Series **1256** (2019) 012018 doi:10.1088/1742-6596/1256/1/012018

Large eddy simulations of floating offshore wind turbine wakes with coupled platform motion

H M Johlas,[1] L A Martínez-Tossas,[2] D P Schmidt,[1] M A Lackner[1] and M J Churchfield[2]

[1]University of Massachusetts Amherst, Dept. of Mechanical and Industrial Engineering, Amherst, MA, USA
[2]National Renewable Energy Laboratory, Golden, CO, USA

E-mail: hjohlas@umass.edu

Abstract. The growing prospect for large farms of floating offshore wind turbines requires a better understanding of wake effects for floating turbines, particularly the differences when compared to fixed-bottom turbine wakes. The increased range of motion of floating platforms can influence wake characteristics, affecting downstream turbines. In this work, large eddy simulations with an actuator line model are used to study downstream wake characteristics of the NREL 5 MW reference turbine mounted on the OC3-UMaine spar platform for several different metocean conditions. The simulations are carried out in the Simulator fOr Wind Farm Applications (SOWFA) coupled with OpenFAST for the platform and turbine motion. The downstream wake characteristics of the floating platform are compared to equivalent fixed-bottom cases for different wind speeds, wave heights, wind-wave alignments, and turbine yaw angles. Overall, the differences in wake shape between floating and fixed platforms are associated with mean platform displacements, while differences in turbulence are associated with time-varying platform motion. However, these observed wake differences between fixed and floating platforms are small, especially for higher wind speeds and lower wave heights.

1 Introduction

Wind turbine wake effects can decrease power output and increase turbine loads, especially for turbines in wind farm arrays. A better understanding of wake physics allows for improved engineering wake models used in design. Wakes of floating offshore wind turbines (FOWTs) are particularly complex because they are generated by a rotor that moves with the floating platform. This study aims to address how downstream wake characteristics differ between fixed and floating platforms and if these differences are sensitive to environmental conditions.

FOWT wakes are difficult to accurately model, due in part to the coupled nature of FOWT rotor aerodynamics and platform motion. To meet this challenge, large eddy simulations (LES) coupled with reasonable platform motions are increasingly used to study FOWT rotor aerodynamics and wakes. For instance, Wang *et al.* [1] compared LES to experimental results for the wake of a multi-turbine platform with prescribed motion. Lyu *et al.* [2] also used LES to briefly examine FOWT behavior for prescribed motion. However, this type of study is limited by prescribed platform motion, which only partially captures the aerodynamic-platform coupling. An improved approach is demonstrated by Lee *et al.* [3], where the responses of waked downstream FOWTs are examined using LES coupled to a turbine dynamics solver.

FOWT wake behavior depends on environmental conditions, just like fixed-bottom turbine wakes. However, most current studies of FOWT wakes do not thoroughly examine the effects

of environmental conditions like wind speed, wave height, or wind-wave alignment, regardless of methodology [4, 5]. In addition, most existing FOWT research focuses on rotor aerodynamics with some near-wake results, with the exception of Lee *et al.* [3], rather than the mid to far wake where downstream turbines would typically be placed.

In this work, the wake of a spar FOWT is simulated with high-fidelity LES using an actuator line model (ALM), in the Simulator fOr Wind Farm Applications (SOWFA) coupled to the turbine simulator OpenFAST. Fixed and floating platforms are compared for different wind speeds, wave heights, wind-wave alignments, and turbine yaw angles.

2 Model details

Wakes of individual FOWTs are simulated in SOWFA [6], a computational fluid dynamics (CFD) tool developed by the National Renewable Energy Laboratory (NREL) based on the OpenFOAM toolbox [7]. The SOWFA simulations of the wake and surrounding atmospheric boundary layer (ABL) flow include an ALM for the turbine rotor, loosely coupled with NREL's aeroelastic turbine simulator OpenFAST v1.0.0 [8] for the motion of the rotor, tower, and platform. OpenFAST's submodules model the effects of the hydrodynamics, mooring lines, and turbine controllers on the turbine motion. The SOWFA-OpenFAST model used in this work is briefly described below, with a more extensive description provided by Churchfield *et al.* [9]. Past validation and verification of the SOWFA framework includes recent work by Doubrawa *et al.* [10], Martínez-Tossas *et al.* [11], Mirocha *et al.* [12], and Churchfield *et al.* [13], with Fleming *et al.* [14] summarizing prior efforts.

The wake simulation workflow in this study consists of three main steps. First, LES of the ABL is performed using SOWFA for a large domain with no turbine, which develops the wind shear profile and large turbulence structures within the ABL. Second, this "precursor" simulation is continued for additional simulation time, which generates and records boundary condition time histories. Third, LES of the turbine wake is performed using SOWFA, coupled to OpenFAST via the rotor ALM. This third SOWFA simulation is initialized using ABL flow field data generated by the first step and uses the boundary condition histories generated during the second step. This workflow is similar to that used by Lee *et al.* [3], among other studies.

2.1 SOWFA

SOWFA solves the filtered incompressible Navier-Stokes equations using a finite-volume method. The momentum equations include Coriolis effects due to the Earth's rotation and incorporate buoyancy effects using the Boussinesq approximation, adding a temperature transport equation [9]. The Deardorff-Lilly one-equation model [15] is used as the LES subgrid-scale model.

The lower boundary is treated using the rough-wall shear stress model of Schumann [16]. Monin-Obukhov similarity theory is used [17] to relate the friction velocity to the flow adjacent to the surface, the surface roughness height z_0, and the surface heat flux, as is common practice in ABL LES [9]. The upper boundary is located in the geostrophic region above the ABL and is therefore modeled as a stress-free, rigid lid. The four side boundary conditions are laterally periodic for precursor ABL simulations, but are inflow or outflow for turbine-wake simulations. The inflow values are based on the recorded boundary conditions from the precursor ABL simulations, while a zero normal gradient condition is used for outflow boundaries.

2.2 Actuator line model

For the turbine-wake simulations, the ALM of Sørenson and Shen [18] is used to model each turbine blade as a line of distributed forces. The drag and lift forces are projected onto the LES flow field as body forces in the momentum equation, using a 3D Gaussian kernel at each blade line element. The width of this Gaussian projection is set to slightly more than twice the local cell size to maintain numerical stability, as Troldborg [19] and Churchfield *et al.* [9] recommend.

The traditional turbine ALM models how the rotor influences the LES flow, but does not

account for the effects of the tower or nacelle. However, work by Santoni *et al.* [20] indicates that including tower and nacelle models can moderately affect the wake up to $6D$ downstream, although their unusually large nacelle may exaggerate the importance of the tower and nacelle. To account for these effects, SOWFA has the capability to include ALM-based tower and nacelle models as described by Churchfield *et al.* [21]. A preliminary study conducted for 8 m/s hub-height wind speed and a fixed platform indicates that the SOWFA tower and nacelle models significantly influence only the near wake, with little effect by $4D$ downstream. Although these models could use improvement [21] and do not appear to affect the far wake, the remaining simulations implement SOWFA's ALM-based tower and nacelle models, in addition to the traditional ALM rotor model.

2.3 OpenFAST

In the coupled SOWFA-OpenFAST turbine simulations, OpenFAST computes the time-varying motion of the turbine blades, tower, and platform. The structural dynamics of the flexible blades and tower are modeled with the ElastoDyn submodule, while variable-speed and blade-pitch control is included using the ServoDyn submodule. The rotor yaw degree of freedom is disabled so that the rotor yaw angle can be set without depending on a yaw controller.

For floating-platform simulations, all six platform degrees of freedom are activated. The hydrodynamic loading on the platform due to a unidirectional, irregular JONSWAP wave train is modeled using the HydroDyn submodule, and the mooring lines are modeled with the MoorDyn submodule. An equivalent fixed-platform turbine is also simulated by disabling the platform degrees of freedom and neglecting hydrodynamic and mooring-line loading. Additional details on the underlying OpenFAST solvers are described by Jonkman and Buhl [22].

3 Simulation setup

3.1 Simulation domains

Two different domains are simulated with SOWFA: a larger one for the precursor ABL simulations and a smaller one with higher mesh resolution for the turbine-wake simulations. Figure 1 illustrates the key features of these two computational domains, including slices through the turbine-wake domain mesh at the rotor plane (for 0^o yaw) and at hub height, colored by instantaneous velocity magnitude. The domain sides and Cartesian mesh are aligned with the cardinal directions, while the average wind flow U_∞ blows from the southwest at 65^o (measured clockwise from north). This angled wind flow direction prevents the turbulent structures from becoming trapped by the periodic boundary conditions in the precursor ABL simulations. The coordinate system is defined so that the x axis is aligned with the average wind flow U_∞, the y axis is aligned with the rotor plane (for 0^o yaw), and the z axis points in the upward direction.

For the precursor ABL simulations, the domain is 3000 m by 3000 m by 1020 m (see Fig. 1), to allow the large-scale ABL turbulent structures to develop. The Cartesian mesh for these ABL simulations consists of 10 m by 10 m by 10 m cells throughout the domain, for a total of 9.2 million cells. For the turbine-wake simulations, the domain size is reduced to 2000 m by 1200 m by 1020 m to reduce computational cost (see Fig. 1). The base cell size remains the same, but two mesh refinement regions are added. First, the mesh is refined twice to 2.5 m cells in the wake region, starting $4D$ upstream of the turbine and ending $10.3D$ downstream. Second, the mesh is refined again to 1.25 m cells in the rotor region, starting $0.5D$ upstream of the turbine and ending $1.5D$ downstream. The mesh slices in Fig. 1 illustrate these refinement regions. In total, the turbine-wake simulation cell count is 18.3 million cells.

The simulated time for the first ABL precursor step is 330 minutes, long enough for the ABL wind shear profile to converge at rotor height. For the turbine-wake simulations, the simulated time is 60 minutes. The second ABL precursor step also has a simulated time of 60 minutes, to generate a full time history of the boundary conditions for the turbine-wake simulations.

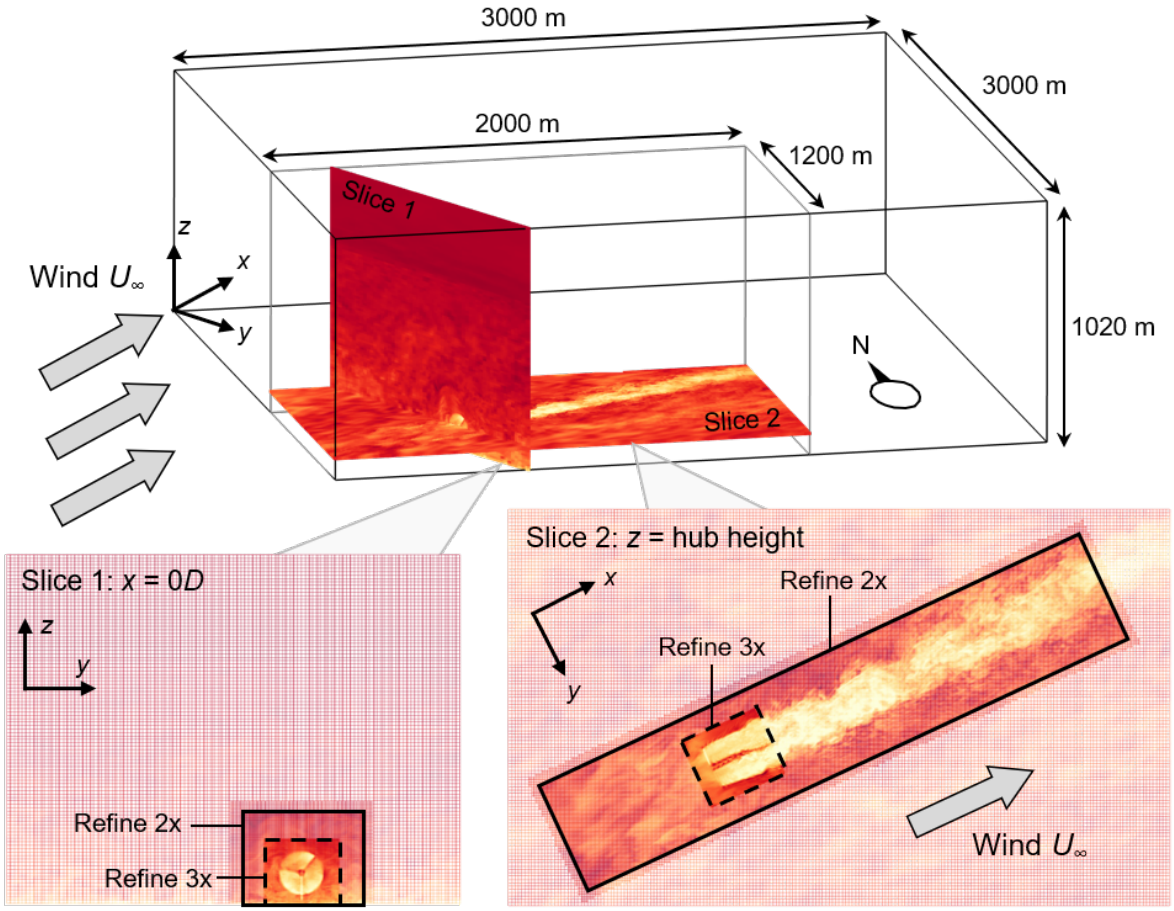

Figure 1. Domains for the atmospheric boundary layer simulations (3000 m x 3000 m x 1020 m) and SOWFA-OpenFAST turbine-wake simulations (2000 m x 1200 m x 1020 m), with an average wind direction from the southwest at 65^o. For the wake domain, mesh slices colored by instantaneous wind speed are shown at the rotor plane ($x = 0D$) and at hub height, including wake and rotor refinement regions (solid and dashed boxes, respectively).

3.2 Case descriptions

In this study, the NREL 5 MW reference turbine [23] mounted on the OC3-UMaine spar buoy platform [24] is simulated for different wind speeds, wave heights, wind-wave alignments, and rotor yaw angles. The OC3-UMaine spar platform is identical to the OC3-Hywind spar platform [25], but with the catenary mooring lines adjusted for 200 m water depth [24].

Two hub-height wind speeds are examined, U_{hh}=8 m/s and U_{hh}=15 m/s, requiring two different precursor ABL simulations. The surface roughness height z_0 is chosen for each U_{hh} based on the Charnock model with $\alpha = 0.011$, as recommended by IEC standard 61400-3 [26]. This model for z_0 is selected because preliminary studies indicate that it produces turbulence intensities that most closely match those measured at the FINO1 platform at z=90 m (hub height) and z=30 m [27]. The wind shear and temperature profiles for both precursor ABL simulations are shown in Fig. 2. All simulations are conducted for a neutral atmosphere with a capping inversion height of z=750 m, as shown by the temperature profiles in Fig. 2.

In addition to varying wind speed, significant wave heights of H_s=4 m and H_s=8 m are compared, with peak spectral periods of T_p=10 s and 14 s, respectively. Wind-wave alignments of ϕ=0^o and 30^o are also compared, where a wind-wave alignment of ϕ=30^o represents waves propagating from the southwest at 35^o. Finally, rotor yaw angles of 0^o and 10^o are compared, where a yaw of 10^o represents a rotor perpendicular to 55^o. The nacelle yaw angle is held

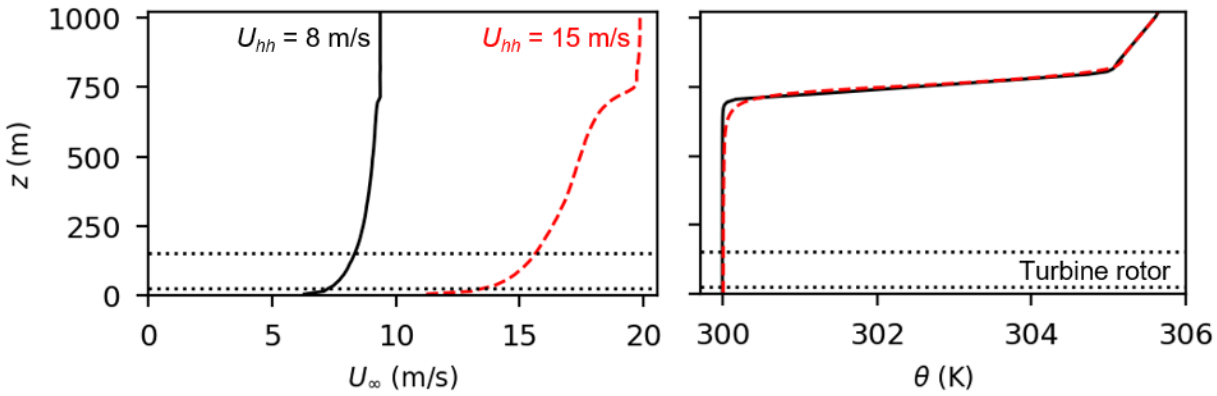

Figure 2. Horizontally averaged wind speed U_∞ and potential temperature θ plotted against elevation z for atmospheric boundary layer cases with hub-height wind speeds U_{hh} of 8 m/s (solid black) and 15 m/s (dashed red). The turbine rotor location is marked by dotted horizontal lines.

constant at the nominal yaw angle, but variations in wind direction and platform yaw motion cause the instantaneous wind-rotor alignment to fluctuate about this average angle.

Floating-platform simulations are conducted for the above parameter values and then compared to equivalent fixed-platform simulations. However, wave height H_s and wind-wave alignment ϕ do not affect fixed-platform simulations because hydrodynamic loading is disabled; so varying H_s or ϕ does not require separate fixed-platform simulations. Starting with a baseline floating-platform simulation with U_{hh}=8 m/s, H_s=8 m, ϕ=0^o, and a yaw of 0^o, eight total cases allow each parameter to be studied individually. Table 1 enumerates each case.

4 Results

To understand how environmental conditions affect the differences between fixed- and floating-platform wakes, each floating case in Table 1 is compared to the equivalent fixed-platform case. The wake is characterized by the horizontal velocity deficit U_d and the turbulent kinetic energy (TKE), which are averaged over 50 minutes, neglecting the first 10 minutes of turbine start-up.

Figures 3 and 4 plot the wake velocity deficit U_d against elevation z and cross-stream coordinate y at downstream locations of x/D=1, 3, 6, and 9. The top row compares the fixed-platform case with U_{hh}=8 m/s and 0^o yaw (case 1) to similar floating-platform cases (cases 2–4) with different wave heights H_s and wind-wave alignments ϕ. The middle row compares the fixed and floating cases with U_{hh}=8 m/s and 10^o yaw (cases 5–6). The bottom row compares the fixed and floating cases with U_{hh}=15 m/s and 0^o yaw (cases 7–8).

Case	U_{hh} (m/s)	TI_{hh} (%)	Yaw (°)	H_s (m)	φ (°)	Platform	C_T
1	8	4.1	0	--	--	Fixed	0.752
2	8	4.1	0	8	0	Floating	0.746
3	8	4.1	0	4	0	Floating	0.744
4	8	4.1	0	8	30	Floating	0.745
5	8	4.1	10	--	--	Fixed	0.742
6	8	4.1	10	8	0	Floating	0.737
7	15	5.0	0	--	--	Fixed	0.255
8	15	5.0	0	8	0	Floating	0.253

Table 1. Simulation cases listed by hub-height wind speed U_{hh}, ambient hub-height turbulence intensity TI_{hh}, rotor yaw angle, significant wave height H_s, wind-wave alignment ϕ, and rotor thrust coefficient C_T. Platform type indicates if platform degrees of freedom are enabled.

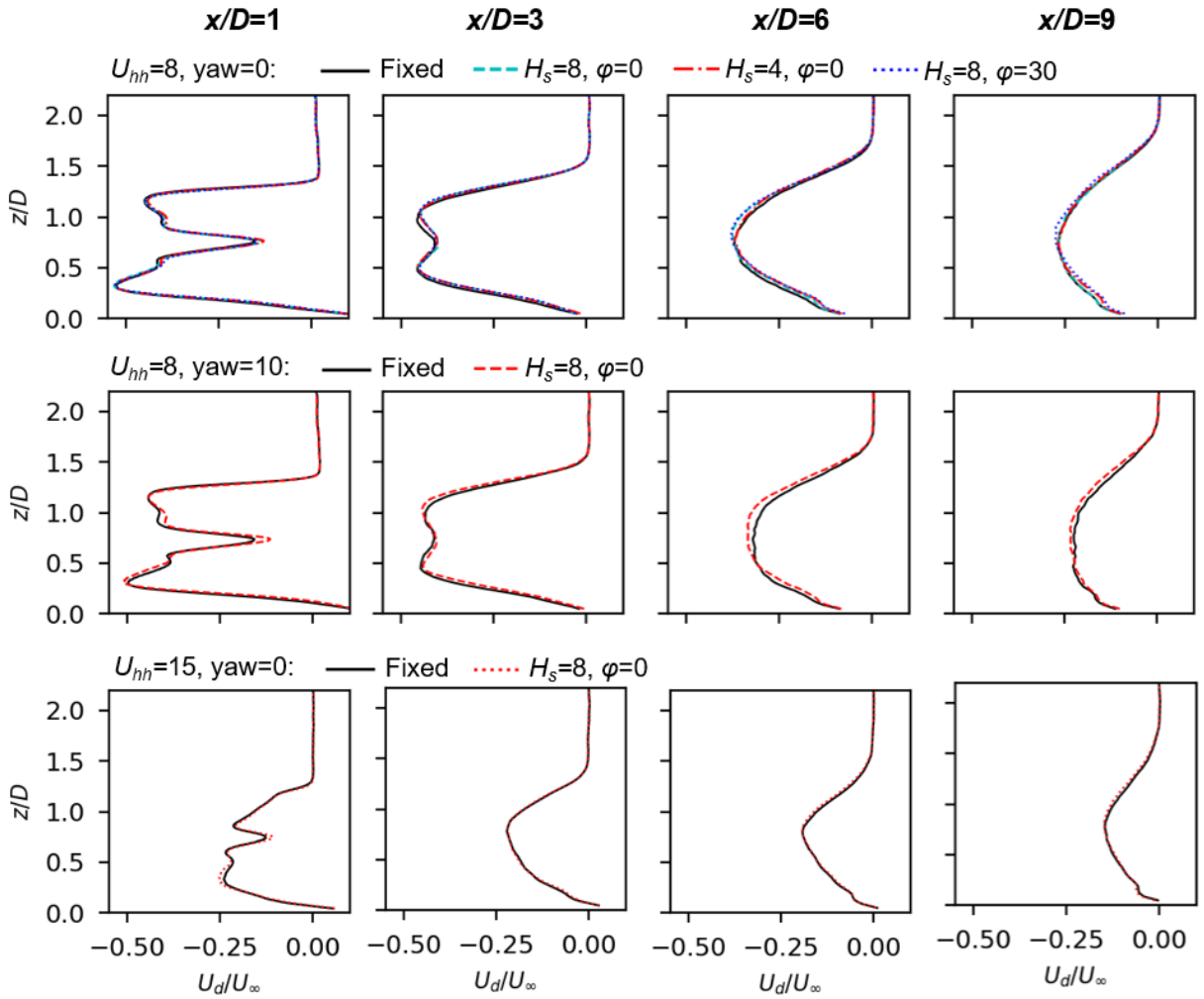

Figure 3. Temporally averaged wake velocity deficit U_d plotted against elevation z at different downstream locations x. Fixed and floating platforms are compared for different wave heights H_s (top), wind-wave alignments ϕ (top), rotor yaw angles (middle), and wind speeds U_{hh} (bottom).

As expected, all wake deficits recover with downstream distance, with the higher wind speed cases recovering faster, partially due to their slightly higher ambient turbulence intensities TI_{hh} and lower thrust coefficients C_T (see Table 1). The deficit profiles in the yawed cases are slightly distorted due to the wake veer caused by the yawed rotor, as expected. In general, floating- and fixed-platform wakes are very similar in shape. As illustrated in Fig. 4, the floating-platform wake deficits are nearly identical to the fixed-platform wake deficits in the cross-stream direction, especially as the distance downstream increases. However, the wake deficit elevation profiles in Fig. 3 show that the floating-platform wakes are generally deflected upward compared to the fixed platform, though this effect is reduced for higher wind speeds or lower wave heights.

Figures 5 and 6 plot the TKE profiles in the wake, in a manner similar to Figs. 3–4. The high-turbulence regions at the blade tips and nacelle decay downstream, with faster recovery for the higher wind speed cases (again, see C_T and TI_{hh} in Table 1). As with the wake deficit, the fixed and floating platforms produce similar TKE profiles. However, the floating platforms produce increased TKE in the wake shear layer compared to the fixed cases, though this effect is lessened for smaller wave heights and higher wind speeds (see in particular Fig. 6).

To better understand how platform motion translates into the wake characteristics displayed in Figs. 3–6, the platform displacements for each floating case are reported in Fig. 7. The average

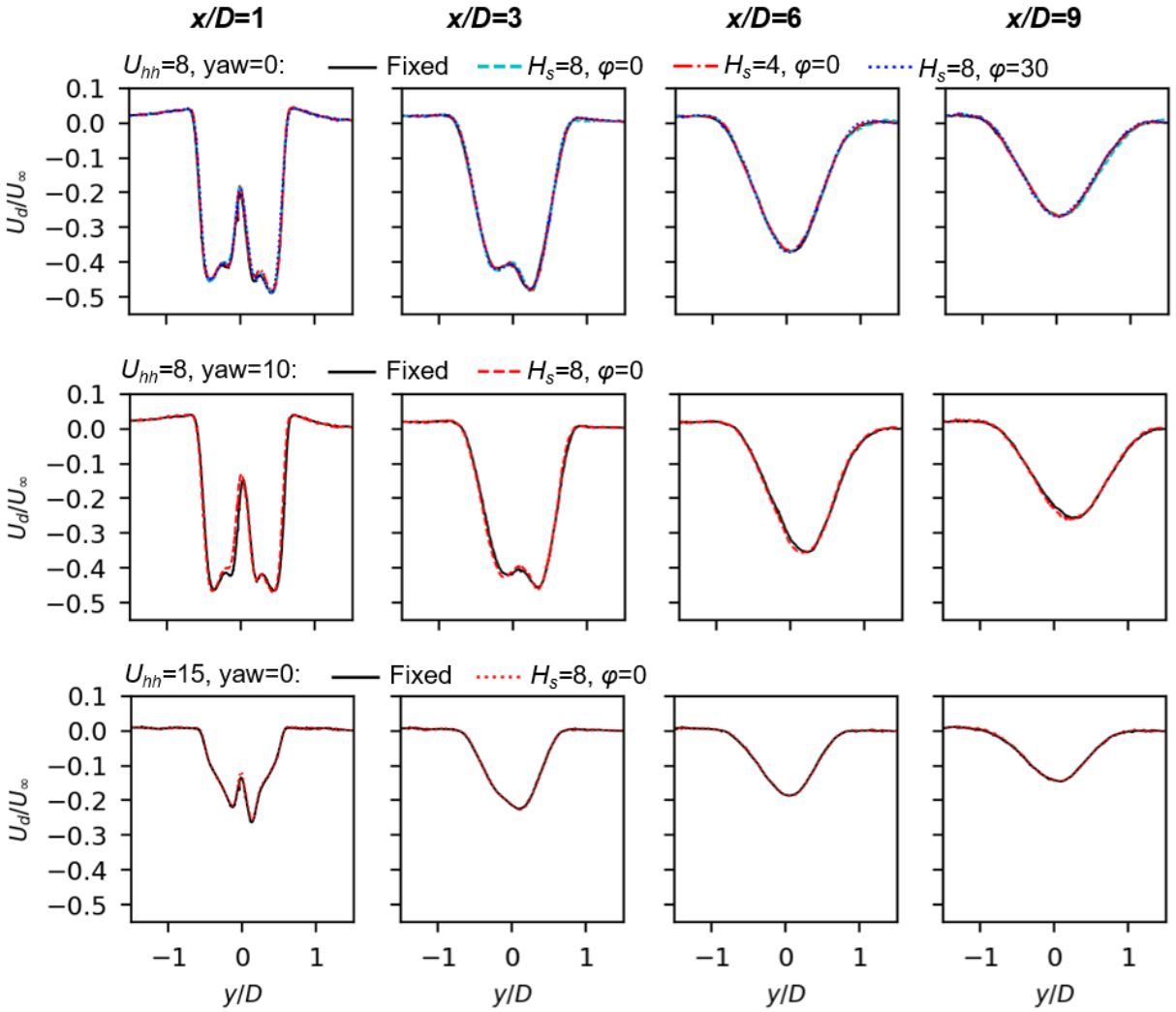

Figure 4. Temporally averaged wake velocity deficit U_d plotted against cross-flow coordinate y at different downstream locations x. Refer to Fig. 3.

displacement over the simulation is reported, as well as the root-mean-square, minimum, and maximum of the time-varying displacement, for each degree of freedom. In Fig. 7, the large mean surge and pitch displacements are caused by the rotor aerodynamic thrust, which increases with wind speed. As expected, the smaller wave height produces less time variation (smaller root-mean-square) in all degrees of freedom. Also, the larger wind-wave misalignment increases the time variation (larger root-mean-square), especially in sway, roll, and yaw.

Based on Figs. 3 and 7, the floating-platform wakes are deflected upward due to the mean platform pitch, as observed in other studies [3, 5]. This vertical deflection is similar to the well-known horizontal wake veer due to rotor yaw. Also, the mean platform surge may explain the slight differences in wake deficit shape at x/D=1: x is measured from a 0 m surge, so that the floating platform's x/D=1 (as reported) is effectively slightly upstream compared to the fixed platform. The importance of this mean surge effect decreases farther downstream.

In addition, based on Figs. 5–7, the increased TKE in the wake shear layer for floating platforms is associated with time-varying platform motion. More platform movement results in more rotor motion, which triggers instability in the wake shear layer faster than in fixed-platform cases. This idea is supported by the H_s=4 m case, where smaller time-varying platform motions

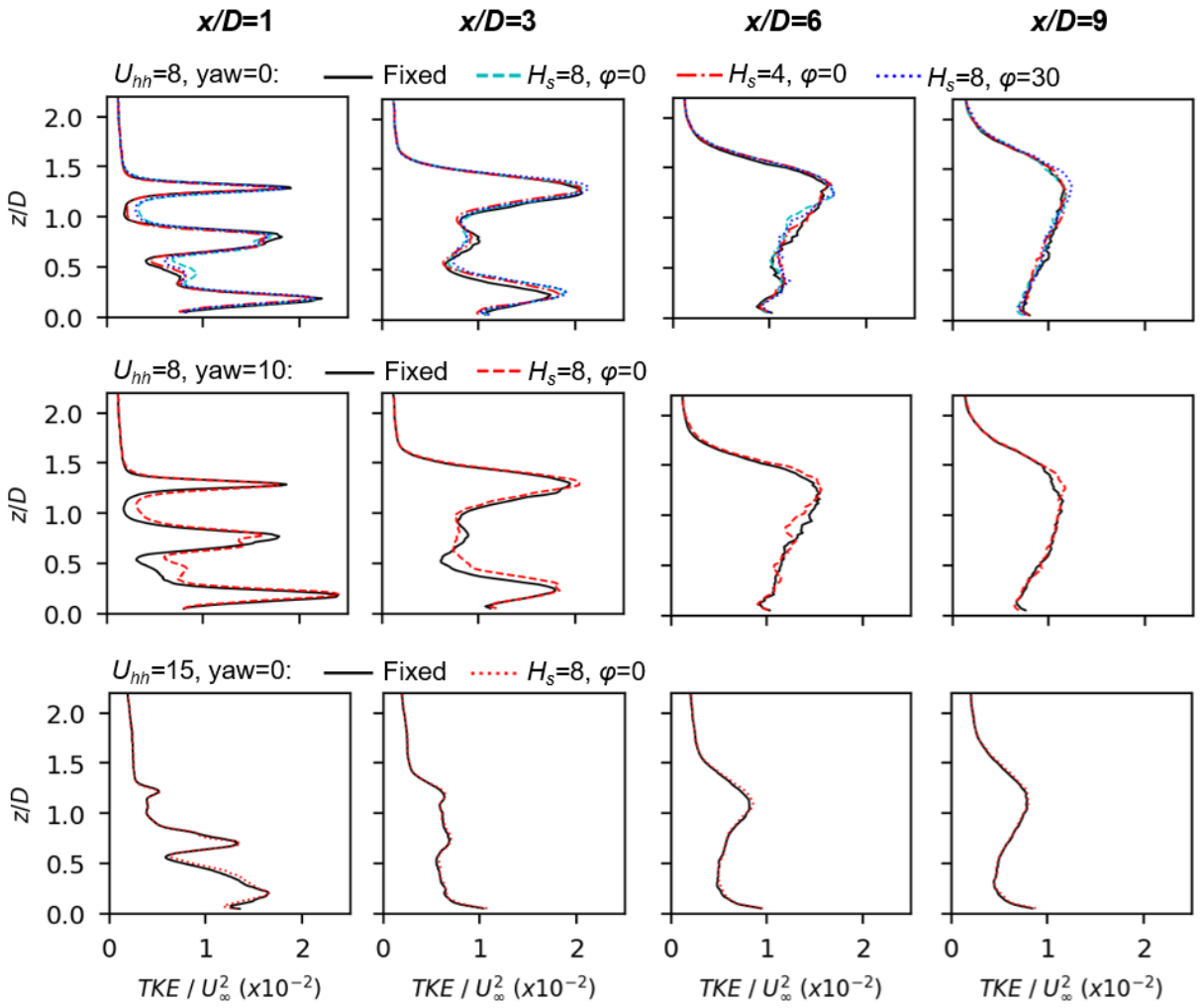

Figure 5. Temporally averaged turbulent kinetic energy plotted against elevation z at different downstream locations x. Refer to Fig. 3.

cause smaller increases in TKE in the wake shear layer.

Overall, Figs. 3–7 indicate that the wake deficit shape is altered by mean platform displacements, specifically shifting the elevation of the peak wake deficit upwards by up to 10%. Also, peak TKE in the wake shear layer is increased up to 6% due to time-varying platform motion. These effects are relatively small in this study, especially for higher wind speeds and lower wave heights. However, because the platform motion is on the order of the simulation cell size, it is unclear if this study adequately resolves the full effects of floating-platform motion on the wake. Although higher mesh resolution remains computationally prohibitive, sufficiently high-resolution data from experiments or field measurements are also difficult to obtain.

5 Conclusions

For the simulated conditions, FOWT wakes have similar characteristics to fixed-platform wakes. Small differences in wake shape are associated with mean platform displacements, particularly a 5–10% upward deflection of the wake due to mean platform pitch. In contrast, variations in turbulence are associated with time-varying platform motions, particularly a 1–6% increase in peak TKE in the wake shear layer. These differences persist into the far wake 6 to 9D downstream, but are reduced for higher wind speeds or lower wave heights. Rotor yaw angle and

wind-wave alignment only minimally affect the differences between fixed- and floating-platform wakes. Due to mesh resolution limitations, these results may not capture all floating-platform wake effects. Future work will address whether these small but non-negligible wake differences produce significant effects on the power output or mechanical loads of a downstream turbine.

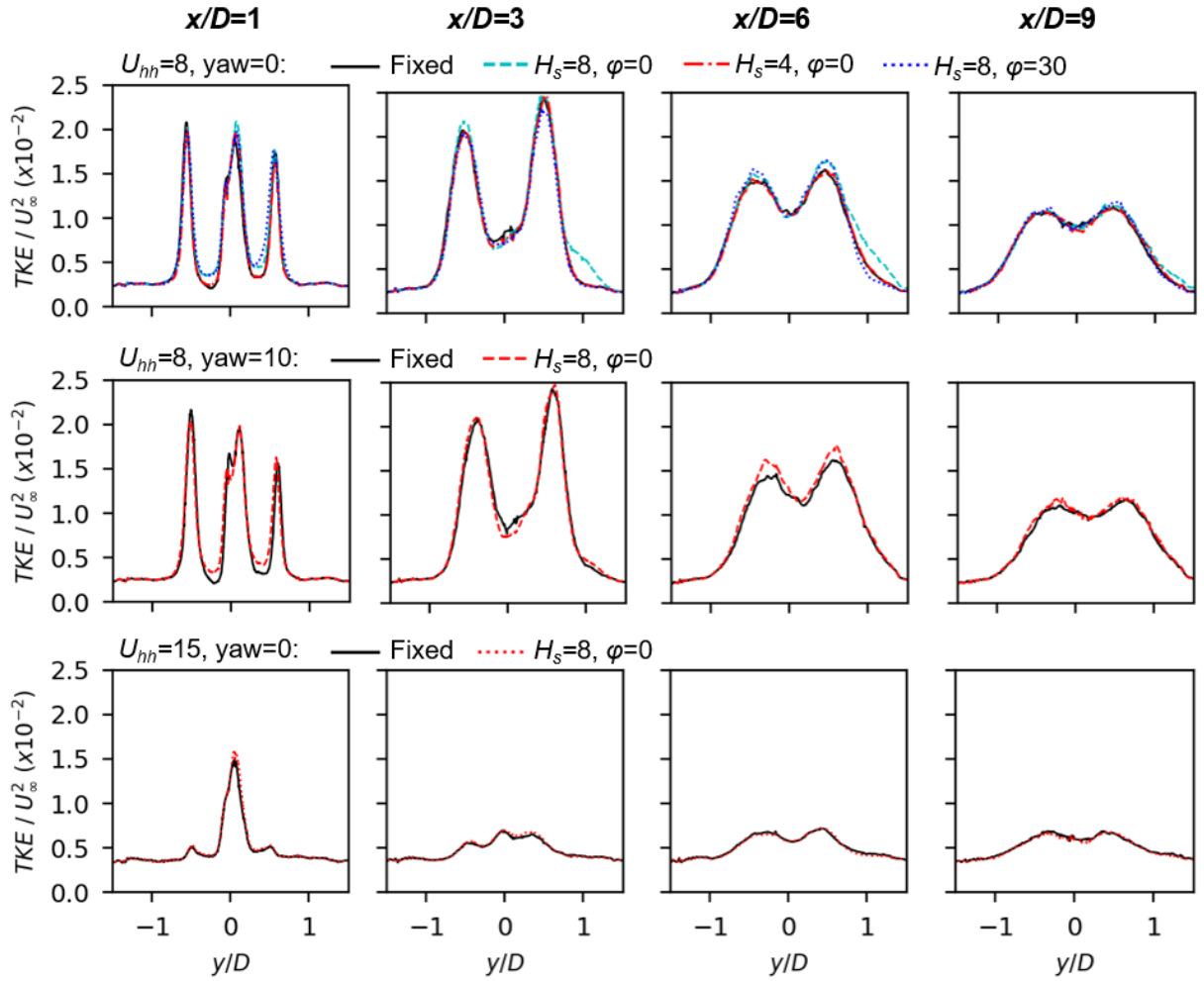

Figure 6. Temporally averaged turbulent kinetic energy plotted against cross-flow coordinate y at different downstream locations x. Refer to Fig. 3.

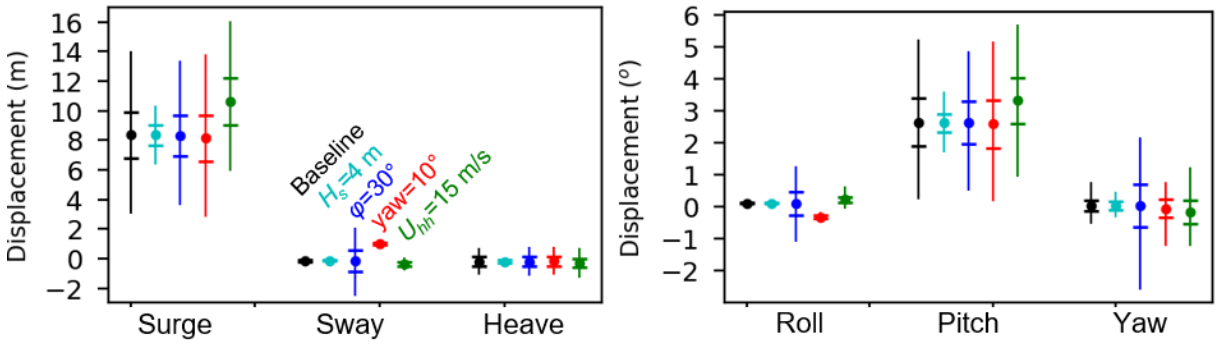

Figure 7. Floating-platform displacements in each degree of freedom, including displacement mean (circles), root-mean-square (horizontal bars), and minimum-maximum (vertical lines). The baseline floating simulation (case 2 in Table 1) is compared to the other floating cases.

Acknowledgments
This research is funded by a National Science Foundation Graduate Research Fellowship, grant #1451512. This work used the Extreme Science and Engineering Discovery Environment (XSEDE) funded by National Science Foundation grant #ACI-1548562, as well as National Renewable Energy Laboratory computational resources sponsored by the U.S. Department of Energy Office of Energy Efficiency and Renewable Energy. This work was authored in part by the National Renewable Energy Laboratory, operated by Alliance for Sustainable Energy, LLC, for the U.S. Department of Energy (DOE) under Contract No. DE-AC36-08GO28308. Funding provided by the U.S Department of Energy Office of Energy Efficiency and Renewable Energy Wind Energy Technologies Office. The views expressed in the article do not necessarily represent the views of the DOE or the U.S. Government. The U.S. Government retains and the publisher, by accepting the article for publication, acknowledges that the U.S. Government retains a nonexclusive, paid-up, irrevocable, worldwide license to publish or reproduce the published form of this work, or allow others to do so, for U.S. Government purposes.

References
[1] Wang J, Wang C, Castañeda O D, Campagnolo F and Bottasso C L 2018 *J. Phys.: Conf. Ser.* **1037** 072032
[2] Lyu P, Park S G, Shen L and Li H 2018 *Proc. of the ASME 1st Int. Offshore Wind Technical Conf. (San Francisco, CA)* IOWTC2018-1046
[3] Lee S, Churchfield M, Driscoll F, Sirnivas S, Jonkman J, Moriarty P, Skaare B, Nielsen F and Byklum E 2018 *Energies* **11**(7) 1895
[4] Sebastian T and Lackner M 2012 *Energies* **5**(4) 968–1000
[5] Rockel S, Peinke J, Hölling M and Cal R 2017 *Renewable Energy* **112** 1–16
[6] Churchfield M and Lee S 2015 NWTC information portal: SOWFA (National Renewable Energy Laboratory) URL `https://nwtc.nrel.gov/SOWFA`
[7] OpenCFD Ltd 2018 OpenFOAM: The open source CFD toolbox URL `https://www.openfoam.com`
[8] Jonkman J and Sprague M 2018 NWTC information portal: OpenFAST (National Renewable Energy Laboratory) URL `https://nwtc.nrel.gov/OpenFAST`
[9] Churchfield M J, Lee S, Michalakes J and Moriarty P J 2012 *J. Turbul.* **13** N14
[10] Doubrawa P, Martínez-Tossas L A, Quon E, Moriarty P and Churchfield M J 2018 *J. Phys.: Conf. Ser.* **1037** 072053
[11] Martínez-Tossas L A, Churchfield M J, Yilmaz A E, Sarlak H, Johnson P L, Sørensen J N, Meyers J and Meneveau C 2018 *J. Renewable Sustainable Energy* **10** 033301
[12] Mirocha, J D *et al* 2018 *Wind Energy Science* **3** 589–613
[13] Churchfield M J, Lee S, Moriarty P J, Hao Y, Lackner M A, Barthelmie R, Lundquist J K and Oxley G 2015 *33rd Wind Energy Symp., AIAA Scitech Forum (Kissimmee, FL)* AIAA2015-0724
[14] Fleming P A, Gebraad P M O, Lee S, van Wingerden J W, Johnson K, Churchfield M, Michalakes J, Spalart P and Moriarty P 2014 *Renewable Energy* **70** 211–8
[15] Moeng C H 1984 *J. Atmos. Sci.* **41**(13) 2052–62
[16] Schumann U 1975 *J. Comput. Phys.* **18**(4) 376–404
[17] Monin A S and Obukhov A M 1954 Basic laws of turbulent mixing in the atmospheric surface layer *Transactions of the Geophysics Institute of the Academy of Sciences of the USSR* **24** 163–87
[18] Sørensen J N and Shen W Z 2002 *J. Fluids Eng.* **124**(2) 393–9
[19] Troldborg N 2009 *Actuator Line Modeling of Wind Turbine Wakes* (Technical University of Denmark, thesis)
[20] Santoni C, Carrasquillo K, Arenas-Navarro I and Leonardi S 2017 *Wind Energy* **20** 1927–39
[21] Churchfield M J, Lee S, Schmitz S and Wang Z 2015 *33rd Wind Energy Symp., AIAA Scitech Forum (Kissimmee, FL)* AIAA2015-0214
[22] Jonkman J M and Buhl M L 2005 *National Renewable Energy Laboratory Report* NREL/TP-500-38230
[23] Jonkman J, Butterfield S, Musial W and Scott G 2009 *National Renewable Energy Laboratory Report* NREL/TP-500-38060
[24] Robertson A N and Jonkman J M 2011 *Proc. of the 21st Int. Offshore and Polar Engineering Conf. (Maui, HI)* ISOPE-I-11-204
[25] Jonkman J 2010 *National Renewable Energy Laboratory Report* NREL/TP-500-47535
[26] International Electrotechnical Commission 2009 *IEC 61400-3 Wind Turbines – Part 3: Design Requirements for Offshore Wind Turbines*
[27] Türk M and Emeis S 2010 *J. Wind Eng. Ind. Aerodyn.* **98**(8–9) 466–71